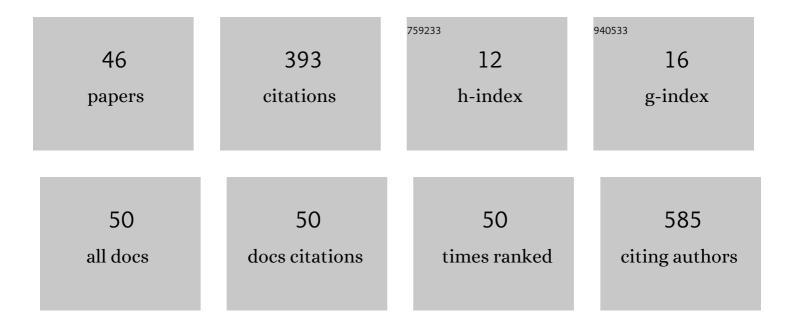
Inmaculada Ãlvarez-Serrano

List of Publications by Year in descending order

Source: https://exaly.com/author-pdf/7831925/publications.pdf Version: 2024-02-01



#	Article	IF	CITATIONS
1	Influence of MnO2-Birnessite Microstructure on the Electrochemical Performance of Aqueous Zinc Ion Batteries. Applied Sciences (Switzerland), 2022, 12, 1176.	2.5	4
2	Stable Manganeseâ€Oxide Composites as Cathodes for Znâ€Ion Batteries: Interface Activation from In Situ Layer Electrochemical Deposition under 2ÂV. Advanced Materials Interfaces, 2022, 9, .	3.7	12
3	Assessing the Electrochemical Performance of Different Nanostructured CeO2 Samples as Anodes for Lithium-Ion Batteries. Applied Sciences (Switzerland), 2022, 12, 22.	2.5	3
4	AgSn[Bi1â^'xSbx]Se3: Synthesis, Structural Characterization, and Electrical Behavior. Crystals, 2021, 11, 864.	2.2	4
5	Î ³ -valerolactone from levulinic acid and its esters: Substrate and reaction media determine the optimal catalyst. Applied Catalysis A: General, 2021, 623, 118276.	4.3	8
6	Exploring multiferroicity in BiFeO3 - NaNbO3 thermistor electroceramics. Journal of the European Ceramic Society, 2021, 41, 7069-7076.	5.7	7
7	Sol-gel synthesis, magnetic and methylene blue adsorption properties of lamellar iron monophosphate KMgFe(PO4)2. Inorganic Chemistry Communication, 2020, 121, 108217.	3.9	6
8	Ni Supported on Natural Clays as a Catalyst for the Transformation of Levulinic Acid into γ-Valerolactone without the Addition of Molecular Hydrogen. Energies, 2020, 13, 3448.	3.1	10
9	Low temperature conversion of levulinic acid into γ-valerolactone using Zn to generate hydrogen from water and nickel catalysts supported on sepiolite. RSC Advances, 2020, 10, 20395-20404.	3.6	7
10	New dielectric anomalies in the A-site highly deficient NaxNbO3 electroceramics. Ceramics International, 2020, 46, 16770-16780.	4.8	12
11	Î′â€MnO ₂ Nanofibers: A Promising Cathode Material for New Aluminumâ€Ion Batteries. ChemElectroChem, 2020, 7, 2102-2106.	3.4	19
12	Synthesis, crystal structure and charge-distribution validation of a new alluaudite-type phosphate, Na _{2.22} Mn _{0.87} 1n _{1.68} (PO ₄) ₃ . Acta Crystallographica Section E: Crystallographic Communications, 2020, 76, 1369-1372.	0.5	2
13	Green synthesis of cavity-containing manganese oxides with superior catalytic performance in toluene oxidation. Applied Catalysis A: General, 2019, 582, 117107.	4.3	8
14	Structural and electrical properties of cobalt-doped 4H- \$mathrm{SrMnO}_{3-delta}\$ SrMnO 3 - δ perovskites obtained by the hydrothermal method. European Physical Journal Plus, 2018, 133, 1.	2.6	0
15	Synthesis and transport properties of p -type lead-free AgSn m SbSe 2 Te m thermoelectric systems. Materials Chemistry and Physics, 2018, 211, 321-328.	4.0	4
16	Focusing on Relevant Features Governing the Electrochemical Behavior of Li (4―x)/3 Ti (5â€2 x)/3 Cr x O 4 Electrode Material. ChemElectroChem, 2018, 5, 1559-1568.	3.4	1
17	New Fe2O3-Clay@C Nanocomposite Anodes for Li-Ion Batteries Obtained by Facile Hydrothermal Processes. Nanomaterials, 2018, 8, 808.	4.1	12
18	Dielectric response and thermistor behavior of lead-free x NaNbO3 - (1-x) BiFeO3 electroceramics. Ceramics International, 2018, 44, 18560-18570.	4.8	16

#	Article	IF	CITATIONS
19	Eco-Friendly Cavity-Containing Iron Oxides Prepared by Mild Routes as Very Efficient Catalysts for the Total Oxidation of VOCs. Materials, 2018, 11, 1387.	2.9	15
20	Nanoparticulated spinel-type iron oxides obtained in supercritical water and their electrochemical performance as anodes for Li ion batteries. Journal of Alloys and Compounds, 2017, 695, 3239-3248.	5.5	5
21	New mortars fabricated by electrostatic dry deposition of nano and microsilica additions: Enhanced properties. Construction and Building Materials, 2017, 135, 186-193.	7.2	18
22	Substrate-induced dielectric polarization in thin films of lead-free (Sr 0.5 Bi 0.5) 2 Mn 2-x Ti x O 6-δ perovskites grown by pulsed laser deposition. Applied Surface Science, 2017, 399, 387-395.	6.1	2
23	Lithium-ion full cell battery with spinel-type nanostructured electrodes. Nano Structures Nano Objects, 2017, 11, 88-93.	3.5	11
24	Characterization of SrBiMn2â^'xTixO6 perovskites: Local ordering influence on the dielectric and magnetic response. Ceramics International, 2016, 42, 11889-11900.	4.8	3
25	Structural and dielectric characterization of new lead-free perovskites in the (SrTiO3)–(BiFeO3) system. Ceramics International, 2016, 42, 8962-8973.	4.8	19
26	Dielectric response of ceramic Sr2â^'xBixTi2â^'xFexO6 (0≤â‰⊈.5) perovskites. Journal of Physics and Chemistry of Solids, 2015, 81, 40-49.	4.0	8
27	Mapping Chemical Disorder and Ferroelectric Distortions in the Double Perovskite Compound Sr2-xGdxMnTiO6 by Atomic Resolution Electron Microscopy and Spectroscopy. Microscopy and Microanalysis, 2014, 20, 731-739.	0.4	2
28	Influence of particle sizes on the electronic behavior of ZnxCo1â^'xFe2O4 spinels (x=0.2,0.3). Journal of Alloys and Compounds, 2014, 601, 130-139.	5.5	4
29	Role of morphology in the performance of LiFe0.5Mn1.5O4spinel cathodes for lithium-ion batteries. Dalton Transactions, 2014, 43, 14787-14797.	3.3	12
30	Crystal structure and Mössbauer spectroscopy of a new iron phosphate Mg2.88Fe4.12(PO4)6. Journal of Alloys and Compounds, 2014, 584, 625-630.	5.5	4
31	Versatile electronic behavior of the LixMn3â^'xâ^'yFeyO4 spinels. Journal of Alloys and Compounds, 2013, 577, 269-277.	5.5	4
32	Characterization of nanoparticulated phases in the manganese oxo/hydroxide system obtained in supercritical water: Optimized conditions for selected compositions. Journal of Supercritical Fluids, 2013, 78, 21-27.	3.2	3
33	Electrochemical performance of Li(4â^'x)/3Mn(5â^'2x)/3FexO4 (x = 0.5 and x = 0.7) spinels: effect of microstructure and composition. Dalton Transactions, 2013, 42, 9990.	3.3	5
34	Enhancement of localization phenomena driven by covalency in the SrBiMn1.75Ti0.25O6 manganite. Journal of Alloys and Compounds, 2012, 522, 123-129.	5.5	5
35	Non-symmetric superparamagnetic clusters in the relaxor manganites Sr2â^'xBixMnTiO6 (0 ≤ ≤0.75). Journal of Materials Chemistry, 2012, 22, 11826.	6.7	11
36	Oriented nanocrystals in SrLaMnTiO6 perovskite thin films grown by pulsed laser deposition. Journal of Alloys and Compounds, 2011, 509, 1457-1462.	5.5	8

#	Article	IF	CITATIONS
37	Room temperature electroresistance in Sr2â^'xGdxMnTiO6 perovskites (0≤â‰⊉). Journal of Alloys and Compounds, 2011, 509, 4917-4923.	5.5	12
38	Structural Characterization and Evolution of the Electronic Behavior of New Sr2â´'xGdxMnTiO6 (0≤â‰\$) Perovskites. Journal of the American Ceramic Society, 2011, 94, 269-276.	3.8	4
39	Tuning magnetic critical behaviour in Ti-manganites by doping with vacancies in A-sites: Sr1â^'â–¡ LaMnTiO6â^' (0 <x≤0.15). 130,="" 2011,="" 280-284.<="" and="" chemistry="" materials="" physics,="" td=""><td>4.0</td><td>5</td></x≤0.15).>	4.0	5
40	Tunable Ferrites as Environmentally Friendly Materials for Energyâ€Efficient Processes. Advanced Materials, 2011, 23, 5237-5242.	21.0	12
41	Random spin configurations of Co cations in LaCo1â^'xMgxO3 (0<xâ‰ 9 .20) perovskite oxides: Magnetic and transport properties. Materials Chemistry and Physics, 2010, 120, 387-392.	4.0	6
42	Microstructural Origin of Magnetic and Giant Dielectric Behavior of Sr ₂ MnTiO _{6â^î^} Perovskite Nanocrystals. Journal of the American Ceramic Society, 2010, 93, 2311-2319.	3.8	15
43	Magnetic behaviour governed by Co spin transitions in LaCo _{1â^'<i>x</i>} Ti _{<i>x</i>} O ₃ (0 ⩽ <i>x</i> ⩽ 0.5) perovskite oxide Journal Physics D: Applied Physics, 2008, 41, 195001.	s.2.8	20
44	Transport properties of new Ti manganites: Sr2â^'xLaxMnTiO6(0.25 â‰ ¤ ≤1). Journal Physics D: Applied Physics, 2007, 40, 3016-3023.	2.8	12
45	CMR in a manganite with 50% of Ti in the Mn sites. Solid State Sciences, 2006, 8, 37-43.	3.2	16
46	Structural characterization, electric and magnetic behaviour of Zn-doped manganites. Solid State Sciences, 2004, 6, 1321-1326.	3.2	17